



## *Fgf8* haploinsufficiency results in distinct craniofacial defects in adult zebrafish

R. Craig Albertson<sup>a,\*</sup>, Pamela C. Yelick<sup>b</sup>

<sup>a</sup> Department of Biology, Syracuse University, 130 College Place, Biological Research Labs, Syracuse, NY 13244, USA

<sup>b</sup> Division of Craniofacial and Molecular Genetics, Department of Oral and Maxillofacial Pathology, Tufts University, 136 Harrison Avenue, Boston, MA 02111, USA

Received for publication 13 October 2006; revised 14 March 2007; accepted 19 March 2007

### Abstract

Significant progress has been made toward understanding the role of *fgf8* in directing early embryonic patterning of the pharyngeal skeleton. Considerably less is known about the role this growth factor plays in the coordinated development, growth, and remodeling of the craniofacial skeleton beyond embryonic stages. To better understand the contributions of *fgf8* in the formation of adult craniofacial architecture, we analyzed the skeletal anatomy of adult *ace<sup>ti282a</sup>/fgf8* heterozygous zebrafish. Our results revealed distinct skeletal defects including facial asymmetries, aberrant craniofacial geometry, irregular patterns of cranial suturing, and ectopic bone formation. These defects are similar in presentation to several human craniofacial disorders (e.g., craniosynostosis, hemifacial microsomia), and may be related to increased levels of bone metabolism observed in *ace<sup>ti282a</sup>/fgf8* heterozygotes. Moreover, skeletal defects observed in *ace<sup>ti282a</sup>/fgf8* heterozygotes are consistent with expression patterns of *fgf8* in the mature craniofacial skeleton. These data reveal previously unrecognized roles for *fgf8* during skeletogenesis, and provide a basis for future investigations into the mechanisms that regulate craniofacial development beyond the embryo.

© 2007 Elsevier Inc. All rights reserved.

**Keywords:** Craniofacial; *fgf8*; Asymmetry; Cranial sutures; Morphometrics; Haploinsufficiency

### Introduction

Fibroblast growth factors (Fgfs) are intercellular signaling molecules that figure prominently in the network of signaling pathways that regulate early patterning and development of the pharyngeal skeleton. Specific requirements for Fgfs during craniofacial development include directing the migration, proliferation and survival of cranial neural crest (CNC) cells (Creuzet et al., 2004), formation of the pharyngeal arches (Crump et al., 2004), establishment of polarity in the mandibular arch (Tucker et al., 1999), and regulation of tooth morphogenesis (Jackman et al., 2004).

Fgfs have also been implicated in directing later stages of skeletal development, and in a variety of developmental disorders. In vitro models have demonstrated roles for Fgfs in regulating the differentiation and function of both osteoblasts

(bone-forming cells) and osteoclasts (bone-resorbing cells), consistent with a role for Fgfs in bone growth, turnover, homeostasis, and remodeling (Shimoaka et al., 2002; Valta et al., 2006; Zuo et al., 2004). Research on mis-expression of various Fgf ligands and receptors in mice supports a critical role for Fgf signaling during the development and growth of the bony skeleton (Colvin et al., 1996; Deng et al., 1996; Govindarajan and Overbeek, 2006; Sobue et al., 2005; Valta et al., 2006; Yu et al., 2003). While certain Fgfs and Fgf receptors (Fgfrs) appear to function as positive regulators of bone development (Valta et al., 2006; Yu et al., 2003), others clearly function as negative regulators (Colvin et al., 1996; Deng et al., 1996). Fgf2 has opposite effects on bone formation during pre- and postnatal development – stimulating the production of osteoblasts during early development (Montero et al., 2000), and decreasing bone formation and density at later developmental stages (Sobue et al., 2005). Mutations in *Fgfr1-3* have been implicated in both syndromic and non-syndromic craniosynostoses and skeletal dysplasia disorders including

\* Corresponding author. Fax: +1 315 443 2012.

E-mail address: [rcalbert@syr.edu](mailto:rcalbert@syr.edu) (R.C. Albertson).

Apert, Crouzon, Saethre-Chotzen and Pfeiffer syndromes (reviewed by Nie et al., 2006). These data underscore dynamic and vital roles for Fgf signaling during skeletogenesis.

Here we examine the consequences of *fgf8*-haploinsufficiency on craniofacial architecture in the developmentally tractable zebrafish model. We hypothesized that if Fgf8 plays a critical role in bone formation and growth, then haploinsufficient adult zebrafish will exhibit subtle but distinct craniofacial defects. We found that *ace<sup>ti282a</sup>/fgf8* heterozygous adults exhibit discrete craniofacial asymmetries, altered craniofacial geometry, aberrant cranial suturing, and ectopic bone growth. *Fgf8*-haploinsufficiency also resulted in increased levels of osteoblast and osteoclast activity, consistent with *fgf8* functioning as a negative regulator of bone growth and remodeling in the zebrafish. These data provide novel insight into the functional roles of *fgf8* during skeletogenesis, and provide a foundation for future investigations into the molecular mechanisms that regulate the coordinated formation, growth and remodeling of the craniofacial skeleton.

## Methods

### *Zebrafish breeding and husbandry*

Zebrafish were maintained and bred at 28.5 °C in a 14-h light/10-h dark cycle at the Forsyth Zebrafish Facility. Embryos were collected by natural mating of pair-wise crosses, and maintained at 28.5 °C as described (Westerfield, 1995). For this study we used mutants that carried the *ace<sup>ti282a</sup>* allele, which encodes a point mutation in the splice site following exon 2, causing a frame shift and introduction of a premature stop codon (Reifers et al., 1998). The *ace<sup>ti282a</sup>* allele strongly attenuates Fgf8 signaling (Reifers et al., 1998), however some residual *fgf8* message may be produced in *ace<sup>ti282a</sup>* homozygous mutants (Draper et al., 2001). Heterozygous carriers of the *ace* allele were genotyped by PCR analysis of tail clip DNA using dCAPS primers, bwd394 (5' to 3'): GAGACGGACACATTTGGGAGTCGAG and bwd395 (5' to 3'): AAGTCACAAAAGTGATGACTTTTTCAGATA (Invitrogen, Carlsbad, CA), followed by digestion with the restriction enzyme *EcoRV* (Neff et al., 1998).

### *Staining for bone*

The bony skeletons of adult zebrafish were stained with Alizarin red as described (Potthoff, 1984), with slight modifications. Adult fish between 8 and 12 months of age were fixed overnight in 4% paraformaldehyde (PFA) in phosphate-buffered solution containing 0.1% Tween-20 (Sigma-Aldrich, St. Louis, MO). Fixed specimens were then enzymatically cleared using a trypsin solution containing 1 g of trypsin powder (Sigma-Aldrich, St. Louis, MO) in 30 ml of distilled H<sub>2</sub>O plus 30 ml sodium borate-saturated distilled H<sub>2</sub>O. After clearing, bone tissue was stained in 0.5% KOH with enough aqueous Alizarin red to turn the solution a deep purple. Pigment was then bleached in a 10% H<sub>2</sub>O<sub>2</sub> solution, and specimens were stored in 80% glycerol. Bone was stained in living larval zebrafish using a 0.1 mg/ml solution of the vital stain Quercetin (Sigma-Aldrich, St. Louis, MO), and visualized under UV illumination using a Zeiss M2 Bio stereomicroscope. All bone preparations were photographed using a Zeiss Axiocam digital imaging system mounted to an M2 Bio stereomicroscope (Zeiss), and processed in Adobe Photoshop 7.0.

### *Quantitative shape analyses*

All shape analyses were performed on cleared and stained adult (12 months) zebrafish from the same family (full siblings). Mandibular asymmetry was defined as the deviation (in μm) of the mandibular symphysis from the cranial midline (Fig. 2). Opercle asymmetry was defined as the difference in left and

right opercle centroid size (CS) for each individual. CS is a geometric descriptor of size measured as the square root of the sum of squared distances of a set of landmarks to their centroid. Landmarks used to describe the opercle are illustrated in Fig. 3. The degree of *ace<sup>ti282a/+</sup>* mandibular and opercle asymmetry was compared to that in *+/+* zebrafish using one-way ANOVA. The sidedness of asymmetry was assessed via Chi-square test and ANOVA on phenotypes that fell outside of the 95% confidence interval.

Cranial suture morphology was assessed by measuring the deviation (in μm) of the interfrontal and sagittal sutures from the cranial midline (Fig. 2). One-way ANOVA was used to compare suture morphology in *ace<sup>ti282a/+</sup>* and *+/+* zebrafish. Patterning of the coronal (transverse) suture was also examined in *ace<sup>ti282a/+</sup>* zebrafish, but statistically significant differences were not observed, and these data are not presented.

Craniofacial shape was compared between *ace<sup>ti282a/+</sup>* animals and their homozygous wild-type siblings via landmark-based geometric morphometrics (GM) in tpsRelw 1.42 (Rohlf, 2005). Landmarks used to describe craniofacial geometry are presented in Figs. 3 and 4. Superimposition of landmark data was achieved using a Generalized Procrustes Analysis (GPA) (Gower, 1975; Rohlf and Slice, 1990), which superimposed landmark configurations such that the sum of squared distances between corresponding landmarks was minimized by scaling, translating, and rotating specimens with respect to a mean consensus configuration. We then performed a thin-plate spline (TPS) analysis, which models the form of an infinitely thin metal plate that is constrained at some combination of points (i.e., landmarks) but is otherwise free to adopt a target form in a way that minimizes bending energy (Bookstein, 1991). In morphometrics, this interpolation is applied to a Cartesian coordinate (*x*, *y*) system in which deformation grids are constructed from two landmark configurations (Bookstein, 1991). The total deformation of the thin-plate spline can be decomposed into geometrically orthogonal components based on scale (Rohlf and Marcus, 1993). These components (partial warps) can be localized to describe precisely what aspects of shape are different. A principal component analysis (PCA) was then performed on partial warp scores, formally referred to as relative warp analysis (RWA) (Bookstein, 1996), to identify major axes of shape variation.

### *Whole-mount TRAP and AP staining*

Osteoclast and osteoblast activities were examined in adult (12 months) *ace<sup>ti282a/+</sup>* zebrafish and their homozygous wild-type siblings by assaying the presence of acid and alkaline phosphatase activity, respectively, in the jaws of adult fish.

For detection of tartrate-resistant acid phosphatase (TRAP), adult fish were fixed overnight at 4 °C in 5% neutral formal saline in 10% formalin. The following morning specimens were washed several times in distilled water, and eyes and viscera were removed, followed by decalcification in 10% EDTA in Tris buffer for 24 h. Specimens were then incubated in a tartrate buffer solution [50 mM Na tartrate+0.2 M acetate buffer (0.2 M acetic acid+0.2 M Na acetate), pH 5.5] for 2 h. TRAP activity was detected using a substrate solution containing 25.6% Michaelis veronal–acetate (1.94% sodium acetate·3H<sub>2</sub>O+2.94% sodium barbiturate), 61.3% distilled H<sub>2</sub>O, 5.1% naphthol AS-TR phosphate in *N,N*-dimethylformamide (10 mg/ml), 4% pararosaniline–HCl (2% pararosaniline in 2 N heated HCl), 4% sodium nitrite. The TRAP solution was made no more than 3 h prior to use, and specimens were incubated in this solution for 2 h at room temperature. Afterwards, specimens were washed several times in distilled H<sub>2</sub>O. Tissue was enzymatically cleared using trypsin (1 g trypsin powder in 30 ml H<sub>2</sub>O+30 ml sodium borate saturated H<sub>2</sub>O). Pigment was bleached in 10% H<sub>2</sub>O<sub>2</sub>, and specimens were stored in 80% glycerol.

For identification of osteoblasts, alkaline phosphatase (AP) activity was visualized. Specimens were fixed and eviscerated as described above, and incubated in 0.05 M Tris–maleate buffer pH 8.3 for 1 h. Tris–maleate buffer was made by adding 2.42 g of tris (hydroxymethyl) aminomethane+2.32 g maleic acid to 100 ml H<sub>2</sub>O, adjusted to pH 8.3 with 0.2 M NaOH. Specimens were then transferred to an AP substrate solution containing 0.5 ml (10 mg/ml) naphthol AS-TR phosphate in *N,N*-dimethylformamide, 50 ml Tris–maleate buffer pH 8.3, plus 40 mg diazonium salt (fast blue), and incubated for 1 h. Specimens were cleared in trypsin and H<sub>2</sub>O<sub>2</sub> as described above, and stored in 80% glycerol.

Whole-mount TRAP and AP staining provided a precise and generalized view of bone remodeling in zebrafish. TRAP activity was detected both in osteoclast cells and on bone surfaces that had undergone bone resorption. In particular, TRAP activity was observed in and around regions expected to undergo continuous remodeling, including cranial sutures, fins, scales and sites of muscle and ligamentous attachment (Figs. 1A–D). Similarly, AP staining labeled osteoblast cells with high precision, and was observed in regions predicted to be undergoing ossification and bone growth (Figs. 1E, F).

Specimens were mounted in 80% glycerol and photographed with a Zeiss Axiocam digital imaging system mounted to an M2 Bio stereomicroscope (Zeiss). The relative percent of TRAP and AP staining in the lower jaws of *ace<sup>ti282a/+</sup>* and homozygous wild-type individuals was measured using the histogram tool in Adobe Photoshop 7.0, and compared via one-way ANOVA.

#### Whole-mount *in situ* hybridization (WISH) analysis

WISH analyses were performed on staged embryos using an adapted protocol (Sagerstrom et al., 1996; Thisse et al., 1993). Juvenile and adult zebrafish were collected at different stages, fixed in 4% PFA in phosphate-

buffered solution containing 0.1% Tween-20, and dehydrated in methanol. Specimens were rehydrated, digested with 10 µg/ml proteinase K, and refixed in 4% PFA. Prehybridization was performed at 65 °C for 3 h in 50% formamide, 5× SSC, 0.1% Tween-20, 4.6 mM citric acid, 50 µg/ml heparin, and 500 µg/ml tRNA. Anti-sense riboprobe was synthesized from *fgf8* cDNA (Reifers et al., 1998) and labeled with digoxigenin (Roche Applied Science, Penzberg, Germany). Labeled riboprobe was added directly to the prehybridization mix and allowed to incubate overnight at 65 °C. Washes were performed the following day at 65 °C in graded solutions from 100% hybridization mix to 100% 2× SSC, and then in 0.2× SSC. Specimens and α-dig antibody were pre-blocked at room temperature for at least 3 h in a solution containing 1 part 10% Boehringer blocking reagent dissolved in 1 M maleic acid, 1 part lamb serum, and 3 parts filtered maleic acid buffer (MAB; 100 mM maleic acid, 150 mM NaCl, 0.1% Tween-20, 7.9 g/l NaOH, pH 7.5). After pre-blocking, specimens were transferred to the α-dig antibody solution and blocked overnight at 4 °C. The following morning specimens were washed first in MAB, and then in AP buffer solution (60 mM Tris–HCl pH 9.5, 60 mM NaCl, 30 mM MgCl<sub>2</sub>, and 0.1% Tween-20). Staining was achieved with NBT and BCIP in AP buffer. After staining, specimens were refixed in 4% PFA, dehydrated in 100% methanol overnight to remove background staining, and stored in 80% glycerol.

## Results

### *Fgf8* haploinsufficiency results in craniofacial asymmetries

Mandibular positioning relative to the midline was measured in *ace<sup>ti282a/+</sup>* adult zebrafish and their homozygous wild-type siblings. A significant difference was observed in the deviation of the mandibular symphysis from the cranial midline in *ace<sup>ti282a/+</sup>* ( $n=52$ ) and wild-type ( $n=45$ ) zebrafish ( $F$ -ratio=8.55,  $p=0.0052$ ). On average, deviation in *ace*-zebrafish was twice as much as that observed in wild-type zebrafish (90 and 46 µm, respectively). Sidedness of mandibular asymmetry was determined by comparing heterozygous and homozygous phenotypes that fell outside the 95% confidence interval for each genotype. This comparison was used to control for the effects of extreme phenotypes. The average deviation from the midline was 9.2 µm to the left side (i.e., the left side was smaller than the right) in wild-type zebrafish ( $n=11$ ), which was significantly different from the heterozygous phenotype where the average deviation of the mandibular symphysis was 128.8 µm to the left side ( $n=10$ ) ( $F$ -ratio=4.07,  $p=0.05$ ). Sidedness of mandibular asymmetry in *ace<sup>ti282a/+</sup>* zebrafish was confirmed using a Chi-square goodness of fit test. Of 52 *ace<sup>ti282a/+</sup>* animals analyzed, 10 (19%) exhibited mandibular asymmetries outside the 95% confidence interval (Figs. 2A–C). Eight of the 10 (80%) asymmetric *ace<sup>ti282a/+</sup>* animals presented mandibles skewed to the left side, which is significantly more than what would be expected by chance ( $\chi^2=3.6$ ,  $df=1$ ,  $p=0.05$ ). These data are consistent with mandibular asymmetry having a directional ( $R > L$ ) bias in *ace<sup>ti282a/+</sup>* zebrafish.

Opercle asymmetry was measured by comparing left and right opercle centroid sizes (CS). A significant difference was observed in opercle asymmetry in *ace<sup>ti282a/+</sup>* ( $n=50$ ) and homozygous wild-type ( $n=48$ ) zebrafish ( $F$ -ratio=3.72,  $p=0.058$ ). Sidedness of opercle asymmetry was examined by comparing heterozygous and homozygous asymmetries that fell outside the 95% confidence interval for each genotype. The difference between the left and right sides of

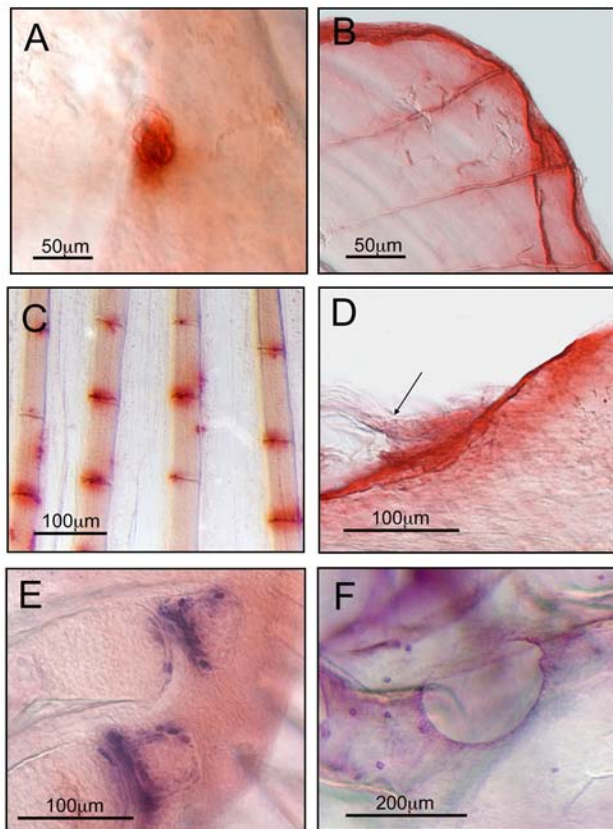


Fig. 1. Images of TRAP (A–D) and AP (E–F) staining in the adult zebrafish. TRAP activity was observed in osteoclasts (A), and in bony structures subjected to continuous growth and remodeling (B–D). An individual osteoclast cell is seen on the surface of the parietal bone (A). TRAP activity was often observed around the distal edges of scales (B). Fin ray joints from all five fins also stained for TRAP, although it was more frequently observed in pectoral and tail fins (pectoral fin, C). Panel D shows TRAP activity on the dorsal surface of the coronoid process of the dentary where the maxillary–mandibular ligament inserts (arrow, anterior is to the left). AP staining of osteoblast cells was observed at sites undergoing endochondral (E) and intramembranous (F) ossification. Endochondral ossification can be seen on pectoral fin radials 4 and 5 (E, dorsal is up). Intramembranous ossification was observed in the lateral line canal on the frontal bone (F, anterior is to the left).

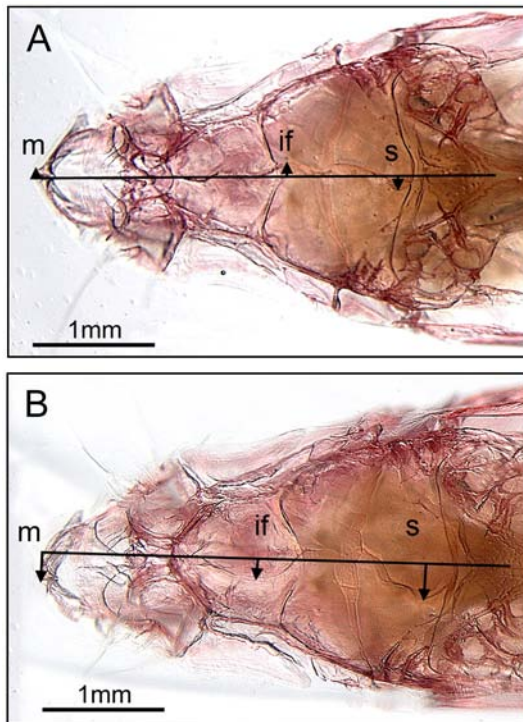


Fig. 2. Mandibular symmetry and cranial suture patterning is altered in  $ace^{ti282a/+}$  zebrafish. The cranial midline was defined as the midline of the neurocranium. In homozygous wild-type zebrafish, the mandibular symphysis (m) was oriented along the cranial midline (A). In  $ace^{ti282a/+}$  animals, however, the mandible exhibited pronounced asymmetry (B). The interfrontal (if) and sagittal (s) sutures in  $ace^{ti282a/+}$  zebrafish also deviated significantly from the midline compared to wild-type siblings ( $F$ -ratio=20.8,  $p<0.0001$ , and  $F$ -ratio=8.36,  $p=0.006$ , respectively).

the opercle was skewed slightly to the right ( $R>L$ ) in wild-type animals ( $n=18$ ,  $L-R=-0.05$ ), which is significantly different from the left-side bias observed in  $ace^{ti282a/+}$  animals ( $n=14$ ,  $L-R=0.230$ ,  $F$ -ratio=3.49,  $p=0.071$ ). Sidedness of opercle asymmetry in  $ace^{ti282a/+}$  zebrafish was confirmed using a Chi-square Goodness of Fit Test. Of 50  $ace^{ti282a/+}$  animals analyzed, 14 (28%) exhibited opercle asymmetries that exceeded at least one 95% confidence interval. Of these, 11 presented cases where the left opercle was larger than the right opercle, which is significantly more than what would be expected by chance ( $\chi^2=4.6$ ,  $df=1$ ,  $p=0.05$ ; Fig. 3). The frequency (e.g., 28%) and bias (e.g.,  $L>R$ ) of opercle size asymmetry in  $ace^{ti282a/+}$  zebrafish is consistent with observations in 7 days post-fertilization (dpf) homozygous recessive  $ace^{ti282a}$  mutants (Albertson and Yelick, 2005), where 28% exhibited pharyngeal bone asymmetries characterized by skeletal elements (typically the opercle) missing from one side of the pharynx. 60% of asymmetric  $ace^{ti282a}$  homozygous recessive mutants were missing bones from the right side of the head. Thus, whereas  $ace^{ti282a}$  mutants exhibited an asymmetry in the presence/absence of the opercle,  $ace^{ti282a}$  heterozygous zebrafish exhibited an asymmetry in the size of the opercle. Both asymmetries have a directional ( $L>R$ ) bias. Notably, the sidedness of opercle and mandibular asymmetries was different in  $ace^{ti282a/+}$  animals. Whether this observation speaks to an

independent or inversely dependent origin of these defects is a question to be investigated in future studies.

Opercle defects in  $ace^{ti282a/+}$  animals mainly affected the relative width of the element (Fig. 3D). This defect, however, was only observed in a percentage of  $ace^{ti282a/+}$  animals (16/50=32%) and was often (but not always) asymmetrically expressed. Irregular opercle shapes observed in  $ace^{ti282a/+}$  zebrafish were distinct from those in  $ace^{ti282a}$  homozygous recessive mutants (Figs. 3E–I). Hyoid arch dermal bones in  $ace^{ti282a}$  larvae were typically either missing, small or generally misshaped ( $n=194$ ). A fraction (~10%) of mutants, however, exhibited more revealing bone phenotypes including fused dermal elements (Fig. 3F), enlarged “opercle-gain” morphologies (Fig. 3G) (Kimmel et al., 2003), and homeosis with both the opercle adopting the shape of the branchiostegal ray (Fig. 3H), and the branchiostegal ray adopting the shape of the opercle (Fig. 3I). These phenotypes are consistent with defects in DV patterning of the hyoid arch (Kimmel et al., 2003). Furthermore these bone defects were only observed in  $ace^{ti282a}$  homozygous recessive larvae—heterozygous larvae exhibited normal dermal bone shapes, suggesting separate roles for  $fgf8$  during pre- and post-larval opercle development.

#### *Ace<sup>ti282a</sup> heterozygous zebrafish exhibit defects in cranial suturing and aberrant craniofacial geometry*

Cranial suture patterns were examined in  $ace^{ti282a/+}$  and homozygous wild-type animals. Specifically, we measured the deviation of interfrontal and sagittal sutures from the cranial midline. In wild-type zebrafish, neither the interfrontal or sagittal sutures deviated significantly from the cranial midline ( $n=25$ ). In  $ace^{ti282a/+}$  zebrafish, however, these sutures exhibited considerable divergence from the cranial midline ( $n=52$ ) (Figs. 2A, D, E). This difference in suture morphology was statically significant for both the interfrontal and sagittal sutures ( $F$ -ratio=20.8,  $p<0.0001$ , and  $F$ -ratio=8.36,  $p=0.006$ , respectively). The coronal and lambdoid (transverse) sutures appeared to be unaffected in  $ace^{ti282a/+}$  animals.

$Ace^{ti282a/+}$  zebrafish also exhibited aberrant craniofacial shape. Landmark-based GM analysis revealed significant differences in the length, height and overall geometry of the craniofacial skeleton between  $ace^{ti282a/+}$  animals and their wild-type siblings. Fourteen landmarks on the oral jaws, suspensorium, pectoral girdle, and skull were used to describe craniofacial architecture (Fig. 4). A relative warp analysis was performed to identify major axes of shape variation.  $Ace^{ti282a/+}$  zebrafish were significantly different from wild-type siblings along principal component (PC) axes 1 and 3 ( $F$ -ratio=8.38,  $p=0.006$ ;  $F$ -ratio=9.94,  $p=0.003$ , respectively), which collectively accounted for 37% of the total variation in craniofacial shape (Fig. 4A). Heterozygous and wild-type animals did not differ in their loadings on PC 2, which explained 17% of the variance and mainly defined the rotation of the upper jaw relative to the skull. This variation was artificially induced due to varying degrees of jaw adduction among samples, and is therefore not biologically

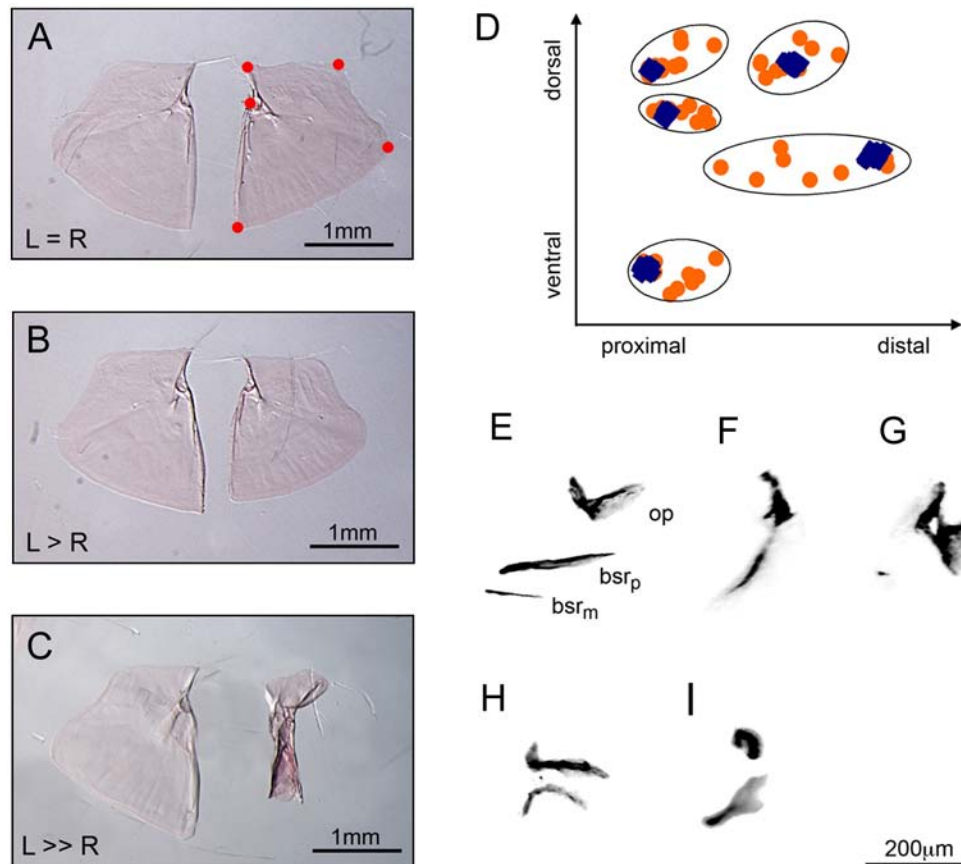


Fig. 3. *Ace*<sup>ti282a/+</sup> zebrafish exhibit asymmetry in opercle size and defects in opercle shape. Opercle size was defined as the square root of the sum of squared distances of the five landmarks depicted in panel A and their centroid (e.g., centroid size). Most mutants possessed left and right opercles that were equivalent in size (A). 28%, however, expressed a pronounced asymmetry in opercle size, with the left side typically larger than the right (B, C). Defective opercle shape in *ace*<sup>ti282a</sup> heterozygous zebrafish mainly affected the width of the opercle (D). Wild-type landmark configurations are depicted as blue diamonds, and *ace*<sup>ti282a/+</sup> configurations are orange circles. Landmarks are the same as in panel A. Very little landmark variation was observed in wild-type zebrafish. Heterozygous animals on the other hand exhibited much greater landmark variation, especially along the proximal–distal axis. Opercle defects in *ace*<sup>ti282a</sup> heterozygotes were distinct from those in *ace*<sup>ti282a</sup> homozygous recessive mutants (E–I). The wild-type configuration of bones from the hyoid arch is shown in the 7 dpf larvae (E). Elements are arranged along the dorsal–ventral (DV) axis with the medial branchiostegal ray (*bsr<sub>m</sub>*) positioned ventrally, the opercle (*op*) positioned dorsally, and the posterior branchiostegal ray (*bsr<sub>p</sub>*) positioned in the middle. Nearly all *ace*<sup>ti282a</sup> mutants were missing the ventral–most branchiostegal ray (*bsr<sub>m</sub>*) and the other two elements were small and misshaped (*n* = 194). However, a percentage of mutant larvae (~10%) exhibited a range of bone morphologies possibly related to defects in DV patterning of the hyoid arch (F–I); these included fused opercle and branchiostegal rays (F), “opercle-gain” phenotypes (Kimmel et al., 2003) (G), and homeotic transformations of the opercle to a branchiostegal ray (H) and visa versa (I).

meaningful. Deformation of shape along the axis that discriminates *ace*<sup>ti282a/+</sup> and wild-type siblings revealed specific differences in the shape of the craniofacial complex. Of particular interest is the deviation in the shape of the frontal bone in *ace*<sup>ti282a/+</sup> zebrafish (purple triangle, Fig. 4B), which is expanded both in length and height relative to the posterior portion of the skull (green line, Fig. 4B). *Ace*<sup>ti282a/+</sup> zebrafish also exhibited concomitant changes in the configuration of the upper jaws (blue triangle, Fig. 4B), and in the relative height of the skull (yellow line, Fig. 4B).

#### *Ace*<sup>ti282a</sup> heterozygous zebrafish exhibit aberrant bone formation

In addition to specific defects in craniofacial shape, *ace*<sup>ti282a/+</sup> zebrafish also exhibited more generalized bone defects, including irregular and ectopic bone formation. These

defects seemed to be limited to the mandible (Fig. 5E), upper jaws, and anterior region of the skull, but until a careful dissection of the articulated craniofacial skeleton is performed we cannot rule out the possibility that other bones might also be affected. The appearance of ectopic bone in *ace*<sup>ti282a/+</sup> animals is consistent with our previous observations of homozygous recessive *ace*<sup>ti282a</sup> mutants, where ectopic bones and cartilages were observed around the developing mandible in approximately 30% of mutants (Albertson, unpublished data).

The intricate configuration of the oral jaw apparatus in bony fishes is constrained by the mechanical requirements of respiration and feeding. These actions impose forces on the craniofacial skeleton that serve to continuously shape and remodel the oral jaw apparatus for optimal performance as the animal grows. We therefore hypothesized that the bone defects observed in *ace*<sup>ti282a/+</sup> zebrafish might relate to the mechanisms that underlie bone growth and remodeling.

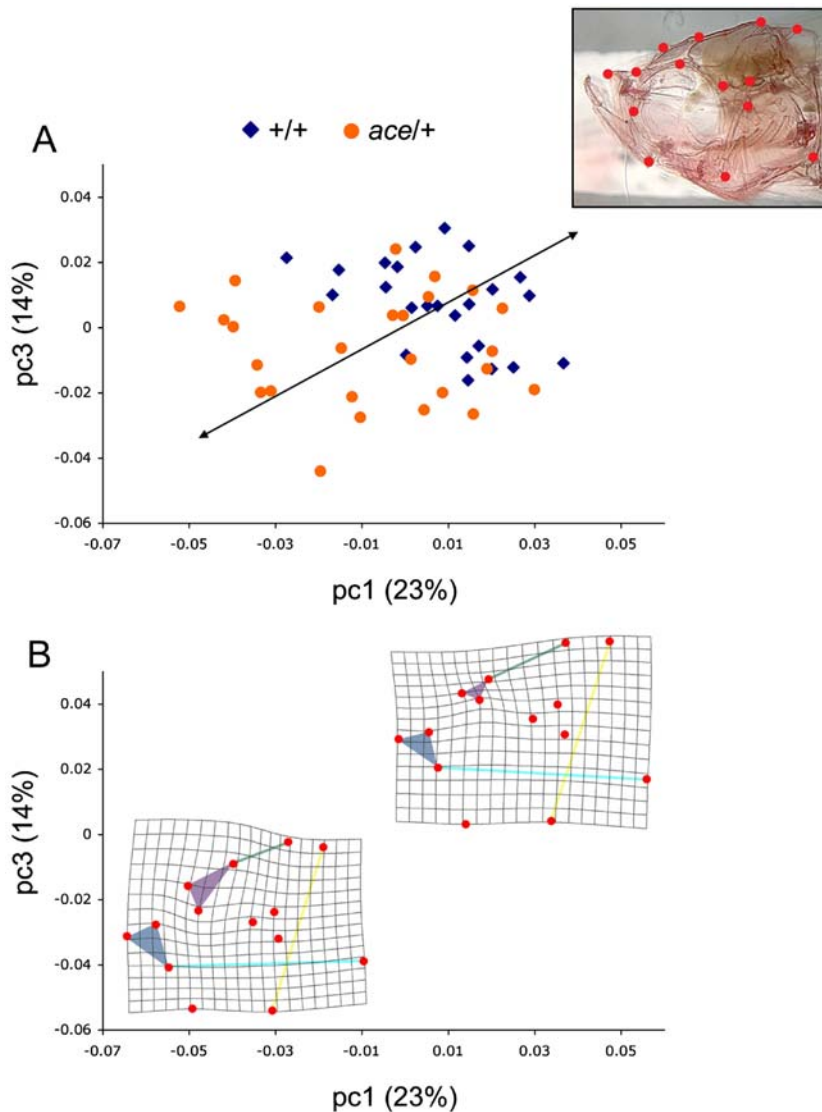


Fig. 4.  $Ace^{ti282a/+}$  zebrafish exhibit aberrant craniofacial geometry. A relative warp analysis revealed two principal component axes that discriminate  $ace^{ti282a/+}$  zebrafish from their wild-type siblings (A). The inset illustrates the position of fourteen landmarks used to describe the craniofacial skeleton in the lateral view. (B), Deformation grids as a function of the axes that differentiate  $ace^{ti282a/+}$  and  $+/+$  individuals.  $Ace^{ti282a/+}$  animals exhibited an expanded frontal region of the skull (purple triangle), relative to the length of the posterior region of the cranium (green line).  $Ace^{ti282a/+}$  zebrafish also exhibited coordinated changes in the configuration of the upper jaws (blue triangle), and in the relative height of the skull (yellow line).

#### *Ace<sup>ti282a</sup>* heterozygotes exhibit increased bone remodeling activity

Tartrate-resistant acid phosphatase (TRAP) and alkaline phosphatase (AP) activities were assessed using whole-mount procedures to identify global patterns of bone remodeling in adult zebrafish (Fig. 1). We observed increased levels of both TRAP ( $n=20$ ) and AP ( $n=20$ ) in the jaws of  $ace^{ti282a/+}$  zebrafish relative to their homozygous wild-type siblings ( $n=20$  each TRAP and AP). TRAP levels were ubiquitously elevated in the mandibles of  $ace^{ti282a/+}$  animals (Figs. 5A and B), whereas elevated AP levels were restricted to distal regions of the jaw (Figs. 5C and D). Elevated levels of TRAP and AP observed in the jaws  $ace^{ti282a/+}$  animals were consistent with the frequent appearance of irregular and ectopic bones (Fig. 5E). TRAP and

AP activities were, on average, two-fold greater in  $ace^{ti282a/+}$  zebrafish than in wild-type zebrafish (Fig. 5F,  $F$ -ratio=30.6,  $p<0.001$ , and G,  $F$ -ratio=7.24,  $p=0.01$ ). Similar increases in TRAP and AP levels were noted for the skull (data not shown). These data suggest that both osteoclast and osteoblast activities are elevated in  $ace^{ti282a/+}$  animals, consistent with *fgf8* functioning as a negative regulator of bone turnover in zebrafish.

Zebrafish development is characterized by extensive allometric growth, making it an excellent model with which to study skeletal remodeling (Witten et al., 2001). However, this attribute also means that skeletal development is particularly dynamic in zebrafish, characterized by shifts in the appearance and location of osteogenic cells depending on the size of the animal (Witten et al., 2001; Albertson, unpublished data). It is also clear that Fgfs play dynamic roles during skeletal

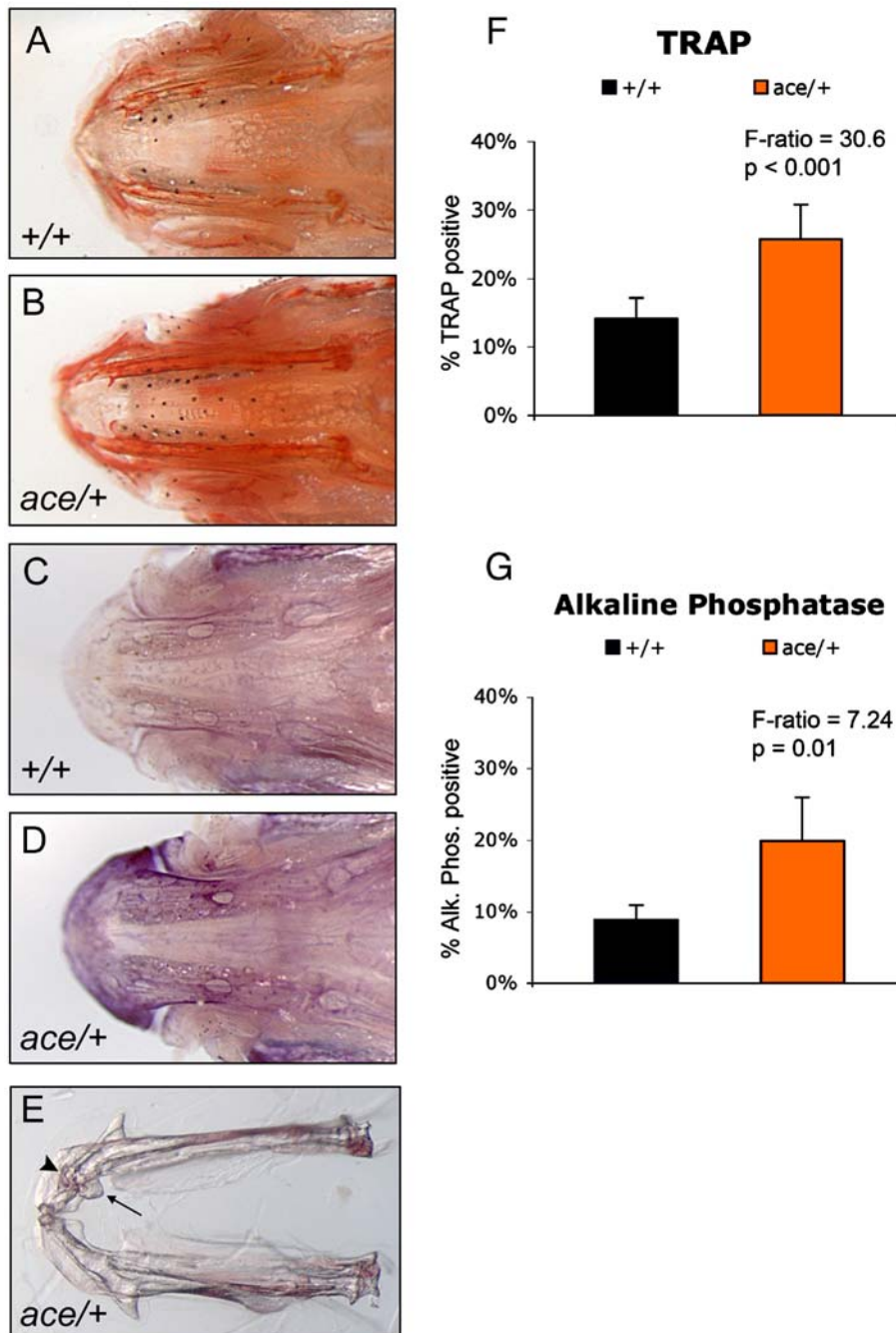


Fig. 5. TRAP and AP activity is elevated in the jaws of  $ace^{ti282a/+}$  zebrafish. A greater proportion of the lower jaw was TRAP positive in  $ace^{ti282a/+}$  animals relative to homozygous wild-types siblings (A, B, F,  $F$ -ratio=30.6,  $p < 0.001$ ).  $ace^{ti282a/+}$  zebrafish also exhibited greater AP activity, localized to the anterior portion of the lower jaw (C, D, G,  $F$ -ratio=7.24,  $p = 0.01$ ). The higher levels of both TRAP and AP activity observed in the mandibles of  $ace^{ti282a/+}$  zebrafish are consistent with the occurrence of aberrant and ectopic bone formation (arrowhead and arrow, respectively, in panel E).

development (Colvin et al., 1996; Deng et al., 1996; Govindarajan and Overbeek, 2006; Sobue et al., 2005; Valta et al., 2006; Yu et al., 2003). In this study, we present a characterization of bone remodeling activities in adult  $ace^{ti282a/+}$  zebrafish, providing insights into *Fgf8* functions at this developmental stage. Additional ongoing studies of zebrafish at multiple developmental stages are currently being performed to define the roles of *Fgf8* signaling in bone formation and remodeling throughout development.

*Fgf8* is expressed in the operculum, oral jaws and cranial sutures

*Fgf8* was expressed in discrete anatomical domains of the mature craniofacial skeleton. Fig. 6 illustrates *fgf8* expression in the head of a 6-month-old zebrafish. Expression was clearly seen in the upper jaw apparatus (black arrow, Fig. 6A), opercular apparatus (white arrow, Figs. 6A and B), cranial sutures (inset, Fig. 6A), and lower jaw (Fig. 6C). *Fgf8*

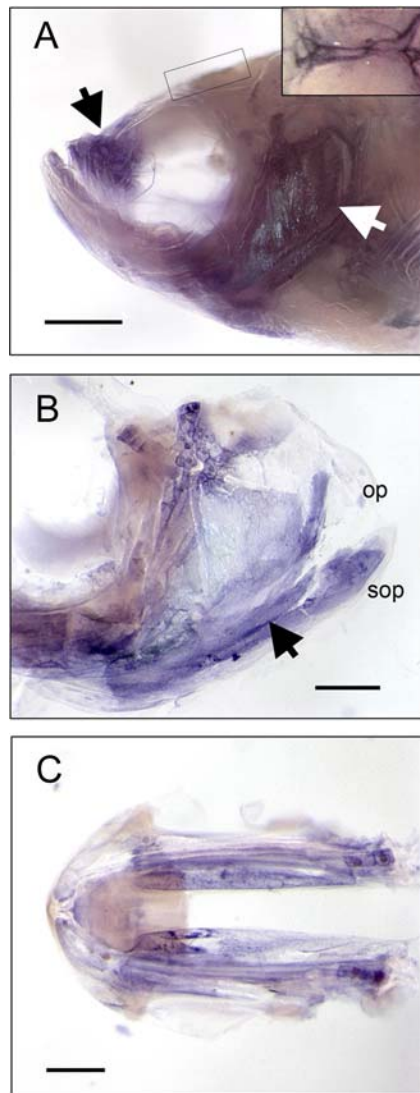


Fig. 6. *Fgf8* mRNA is expressed in distinct anatomical regions of the mature craniofacial skeleton. (A) A 6-month-old wild-type zebrafish head showing *fgf8* expression in the upper jaw apparatus (black arrow), operculum (white arrow), and sagittal suture (inset). Scale bar equals 1 mm. (B) The dissected operculum shows *fgf8* expression throughout the subopercle (sop) and along the proximal–distal surface of the opercle (op) (black arrow). Scale bar=500  $\mu$ m. (C) Expression of *fgf8* is also observed along the ventral surface of the mandible. Scale bar=500  $\mu$ m.

expression around the upper jaws was associated with the premaxilla, maxilla, kinethmoid, and the ethmoid region of the skull. This region of the craniofacial skeleton is a functional “hot spot” comprised of an intricate configuration of bones and ligaments that participate in action of upper jaw protrusion (Hernandez, 2000; Otten, 1983). Forces associated with this action, and imposed on the upper jaws, are likely to play important roles in the growth and remodeling of this region. *Fgf8* expression associated with the opercle was most pronounced at the location where the opercle articulates with the skull and along the ventral/proximal edge of the bone (arrow, Fig. 6B). *Fgf8* was also expressed in the sagittal cranial suture (inset, Fig. 6A), and along the ventral surface of the mandible (Fig. 6C). These expression patterns are consistent

with defects observed in *ace<sup>ti282a/+</sup>* zebrafish, including upregulated osteoblast and osteoclast activities, suggesting a causal relationship between *fgf8* deficiency and observed skeletal defects.

## Discussion

### *Zebrafish skeletogenesis: development beyond the embryo*

Recent efforts to characterize semi- and non-lethal craniofacial mutants in zebrafish have made important contributions to the study of skeletogenesis (Fisher and Halpern, 1999; Fisher et al., 2003; Draper et al., 2003; Elizondo et al., 2005; Albertson and Yelick, unpublished data). Fisher et al. (2003), for example, performed a large-scale ENU-mutagenesis screen for skeletal dysplasia in zebrafish. Using radiography to screen F<sub>1</sub> adult zebrafish for dominant skeletal phenotypes, investigators identified the *chihuahua<sup>dc124</sup>* (*chi*) mutant, which exhibited extensive skeletal defects and mapped to an interval that contained *collagen type 1a (coll1a)* (Fisher et al., 2003). Defects observed in *chi<sup>dc124</sup>* mutants were similar in presentation to humans with osteogenesis imperfecta (OI), a skeletal dysplasia typically caused by mutations in either COL1A1 or COL1A2 (Benusiene and Kucinkas, 2003). A more recent study by Elizondo et al. (2005) characterized the zebrafish *nutrid<sup>124e2</sup>* mutant, which was also identified in an ENU mutagenesis screen for postembryonic phenotypes. The *nutrid<sup>124e2</sup>* mutation mapped to the melastatin-type transient receptor potential (TRPM) channel, *trpm-7* (Elizondo et al., 2005). During embryonic and early larval development *nutrid<sup>124e2</sup>* mutants were similar in size and appearance to wild-type zebrafish, but as adults they exhibited severe growth retardation, skewed body proportions, and a range of skeletal defects (Elizondo et al., 2005). Of particular interest is the altered sequence and timing of skeletal ossification in *nutria-*mutants. An elegant statistical analysis, using a combination Wilcoxon test and logistic regression analysis, showed that *nutrid<sup>124e2</sup>* mutants exhibited significantly accelerated rates of endochondral ossification and correspondingly delayed rates of intramembranous ossification (Elizondo et al., 2005), revealing a complex and vital role for *trpm-7* in the regulation of post-embryonic skeletogenesis. The application of quantitative and statistical analyses to experimental embryology has also facilitated an understanding of the molecular mechanisms contributing to the development of skeletal shapes (Albertson and Yelick, 2004). For example, Kimmel et al. (2003) characterized a phenotypic series of opercle and branchiostegal ray morphologies associated with residual levels of the secreted peptide Endothelin-1 (Edn1). When Edn1 was severely reduced, both the opercle and branchiostegal rays were absent. However, when Edn1 levels were only mildly reduced, the branchiostegal rays were absent but the opercle was expanded in size and altered in shape, resulting in what the authors referred to as an “opercle-gain” phenotype. These loss of function analyses, combined with the ventral pharyngeal arch expression domain of *edn-1* mRNA (Miller et al., 2000), led the authors to posit an Edn1 morphogenic gradient model of hyoid

bone patterning where levels of Edn1 are related to both the DV positioning and size of developing bones. The ventrally positioned branchiostegal rays are closer to the source of Edn1, and therefore more sensitive to its reduction. Lowering Edn1 levels decreases the slope of the gradient leading to a loss of the branchiostegal rays, ventral translocation of the opercle, and expansion of the region of opercle specification (Kimmel et al., 2003).

Hyoid arch bone phenotypes in *ace<sup>ti282a</sup>* larvae were similar to those in *edn-1* mutants as well as to other mutants that may function along the *edn-1* genetic pathway (e.g., *she*, *stu* and *hoo*) (Miller and Kimmel, 2001). These hyoid bone morphologies can be grouped by their putative developmental origin, including fusion of the opercle and posterior branchiostegal ray (Fig. 3F), “opercle-gain” (Fig. 3G), and varying degrees of homeosis (Figs. 3H and I). These data are consistent with *fgf8* functioning to pattern the hyoid arch along the DV axis. Whether *fgf8* operates within or parallel to the *edn-1* pathway remains to be investigated. Notably, opercle bone morphologies in *ace<sup>ti282a</sup>* larvae were distinct from those observed in *ace*-adults, supporting distinct roles for *fgf8* in pre- and post-larval opercle development. During early larval development *fgf8* appears to be necessary for proper DV patterning of the hyoid arch. During post-larval development *fgf8* mRNA is expressed along the ventral–proximal surface of the opercle, and *fgf8* haploinsufficiency results in defects specific to this region, implicating *fgf8* as a regulator of opercle bone growth.

#### *Roles for Fgf signaling in suture formation and craniosynostosis*

Zebrafish cranial sutures are similar in anatomy and development to those in mammals (Quarto and Longaker, 2005), making them a valuable model for the study of human diseases that affect suture formation. Craniosynostosis is a medical condition that involves the premature fusion of the cranial sutures, and affects 1 in 2500 live births (Morriss-Kay and Wilkie, 2005). Mutations have been identified in both syndromic and non-syndromic cases of craniosynostosis, the majority of which occur in *fibroblast growth factor receptor (fgfr) types 1–3* (reviewed by, Morriss-Kay and Wilkie, 2005). These mutations also give rise to several related syndromes, characterized by additional defects in bone formation and growth. Given the genetic epidemiology of craniosynostoses in humans, it is not surprising that Fgf signaling figures prominently in the development and maintenance of cranial sutures. In mammals, as the skull vault grows, osteoblasts at the leading edges of skull bones secrete Fgf ligands, which activate receptors in adjacent undifferentiated mesenchyme. Low levels of Fgf lead to the activation of Fgfr2 and subsequent proliferation of osteoprogenitor cells. As Fgf levels increase, Fgfr2 is downregulated and Fgfr1 is upregulated, leading to a switch from cell proliferation to the overt differentiation of osteoblasts (Iseki et al., 1999). Proper growth of the cranial vault therefore depends on the balance between Fgf-mediated cell proliferation and differentiation along the cranial sutures (Morriss-Kay and Wilkie, 2005).

It remains unclear to what degree zebrafish share the molecular program used to regulate cranial development and growth in mammals. Indeed, the very homology of bones comprising the cranial vault across vertebrate classes is still debated (reviewed in Hanken and Gross, 2005). Nonetheless our results suggest that *fgf8* plays a role in cranial suture development in zebrafish. Specifically, the aberrant suture patterning and the expanded frontal region of the skull observed in *ace<sup>ti282a/+</sup>* zebrafish are consistent with craniosynostosis phenotypes. If cranial suture patterning in zebrafish proves to be similar to that of mammals, continued work in this developmentally tractable system will greatly facilitate our efforts to understand the pathophysiology of craniosynostosis disorders, and the derivation of therapeutically relevant treatments for these syndromes.

#### *A symmetric or asymmetric vertebrate body plan?*

Our data support a molecular genetic basis for directional craniofacial asymmetries, and fit into a larger body of literature seeking to understand the mechanisms that regulate laterality in vertebrates. Directional asymmetries differ from fluctuating asymmetries in that the former produces structures that are biased to either the right- or left-hand side within a population, whereas the latter has no directional bias (right- or left-hand forms occur with equal frequency). Directional asymmetries are generally thought to have a strict genetic basis and develop as a consequence of an internal asymmetric developmental genetic mechanism (i.e., Kawakami et al., 2005). Conspicuous examples of directional asymmetries in vertebrates include the orientation of the heart and the positioning of the visceral organs. Fluctuating asymmetries, on the other hand, do not have a genetic basis and are thought to arise from random perturbations in developmental systems. A multitude of factors have been shown to influence levels of fluctuating asymmetries including environmental quality, hybridization among species, and inbreeding (reviewed by Palmer and Strobeck, 1997). While the mechanisms that regulate the asymmetric development of the brain, heart and viscera have been extensively studied (reviewed by Levin, 2005), we know comparatively little about how directional asymmetries have evolved in normally paired structures (i.e., the narwal’s ‘tusk’, the ears of owls, and the whole body in flatfish). Are the same asymmetric cues being co-opted for the asymmetric development of normally paired structures? Or have other asymmetric signals evolved?

We propose that the vertebrate body plan possesses a fundamental L–R handedness (Albertson and Yelick, 2005), and that the same molecular machinery that establishes the L–R axis during heart and visceral organ development also influences the development of a host of other structures. Our characterization of the zebrafish *ace<sup>ti282a</sup>* mutant demonstrates that deficiency in this growth factor results in conspicuous asymmetric development of the pharyngeal skeleton (data presented above, Albertson and Yelick, 2005). It has also recently been shown that zebrafish lacking retinoic acid (RA) exhibit asymmetric somite development (Kawakami et al.,

2005). In both *fgf8* and RA deficient animals, asymmetric defects were linked to the presence and proper function of Kupffer's vesicle, a ciliated node that mediates laterality information in zebrafish (Albertson and Yelick, 2005; Kawakami et al., 2005). These observations are consistent with a model where Fgf and RA signaling act to buffer the zebrafish embryo from the lateralizing effects of Kupffer's vesicle, leading to bilaterally symmetric segmentation and development of the pharynx and somites (Albertson and Yelick, 2005; Kawakami et al., 2005). Under this model the wild-type function of a handful of factors are necessary for the proper symmetric development of paired structures in an otherwise asymmetric environment.

Additional evidence for a hypothesized asymmetric body plan comes from a range of observations in a variety of disciplines. From a clinical perspective, numerous human birth defects are characterized by craniodental asymmetries, including hemifacial microsomia, Treacher–Collins syndrome, unilateral clefting, Saethre–Chotzen syndrome, Russell–Silver syndrome, and hemifacial hypertrophy. In each of these, spontaneous or inherited defects in the normal developmental program lead to a break in symmetry. Experimentally induced developmental defects can also lead to pronounced asymmetric development of normally paired structures. As discussed above, experimental knock-down of Fgf and RA signaling in zebrafish leads to conspicuous directional asymmetries in the pharynx and somites, respectively. In addition, mice lacking the gene *pitx1* exhibit an asymmetric reduction in hindlimb morphology with the right-side typically more affected than the left (Marcil et al., 2003). This asymmetric phenotype is similar in presentation to patterns of pelvic limb reduction in natural populations of three-spined stickleback (*Gasterosteus*), nine-spined stickleback (*Pungitius*) and Florida manatees (*Trichechus manatus latirostris*) (Shapiro et al., 2006). Moreover in both stickleback genera pelvic reduction mapped to *pitx1* and was associated with alternate *pitx1* expression patterns, suggesting a common genetic mechanism underlying the independent evolution of limb reduction (Shapiro et al., 2004, 2006). “Bookend” (mirror image) phenotypes observed among monozygotic twins, including hair whorl direction, hand preference, vision and hearing defects, and dental patterning, provide another line of evidence for a fundamentally asymmetric body plan that is established very early in development (Levin, 1999). Heritability estimates and mapping studies in humans and mice support a genetic basis for normal directional craniofacial asymmetries (Cassidy et al., 1998; Leamy et al., 2000). Asymmetries in skeletal traits are also a common feature among parents of children with unilateral clefting (AlEmran et al., 1999; McIntyre and Mossey, 2003; Yoon et al., 2003). In fact, the direction of certain facial asymmetries in parents was predictive of the direction of unilateral clefting in their children. This observation suggests that the same loci that underlie natural variation in facial asymmetry are also responsible for clinical asymmetries (Yoon et al., 2003). Finally, several vertebrate taxa have accentuated craniodental asymmetries along the left–right axis (i.e., flatfish, narwals and owls; reviewed by Albertson and Yelick, 2005), consistent with

natural selection targeting an inherently asymmetric developmental program.

Taken together, these data suggest that the vertebrate body plan is only superficially bilaterally symmetrical, and that handedness is inherent to most if not all paired structures. Whether these latent asymmetries are a shared derived character of vertebrates, or an evolutionary consequence of our shared ancestry with echinoderms, which exhibit many peculiar left–right asymmetries that are regulated by many of the same mechanisms as in vertebrates (Cooke, 2004; Duboc et al., 2005; Hibino et al., 2006), remains a topic for debate. What is clear is that further elucidation of the molecular signaling pathways regulating these processes in the zebrafish model, are likely to facilitate our understanding of these basic developmental processes, and to provide a sound basis for the development of educated molecular-based strategies to predict, prevent and/or correct craniofacial asymmetries in humans.

### Acknowledgments

We wish to thank members of the Albertson and Yelick laboratories for thoughtful comments on earlier versions of the manuscript, and Seija Cope for expert zebrafish husbandry. PCY is supported by NIDCR Grants DE12024 and DE12076.

### References

- Albertson, R.C., Yelick, P.C., 2004. Morphogenesis of the jaw: development beyond the embryo. In: Detrich, H.W., Zon, L., Westerfield, M. (Eds.), *The Zebrafish: Cellular and Developmental Biology* (Methods in Cell Biology), vol. 76. Elsevier, San Diego, CA, pp. 437–454.
- Albertson, R.C., Yelick, P.C., 2005. Roles for *fgf8* signaling in left–right patterning of the visceral organs and craniofacial skeleton. *Dev. Biol.* 283, 310–321.
- AlEmran, S.E., Fatani, E., Hassanain, J.E., 1999. Craniofacial variability in parents of children with cleft lip and cleft palate. *J. Clin. Pediatr. Dent.* 23, 337–341.
- Benusiene, E., Kucinskas, V., 2003. COL1A1 mutation analysis in Lithuanian patients with osteogenesis imperfecta. *J. Appl. Genet.* 44, 95–102.
- Bookstein, F.L., 1991. *Morphometric Tools for Landmark Data: Geometry and Biology*. Cambridge University Press, New York.
- Bookstein, F.L., 1996. Combining the tools of geometric morphometrics. In: Marcus, L.F., Corti, M., Loy, A., Naylor, G.J.P., Slice, D.E. (Eds.), *Advances in Morphometrics*. Plenum, New York, pp. 131–151.
- Cassidy, K.M., Harris, E.F., Tolley, E.A., Keim, R.G., 1998. Genetic influence on dental arch form in orthodontic patients. *Angle Orthod.* 68, 445–454.
- Colvin, J.S., Bohne, B.A., Harding, G.W., McEwen, D.G., Ornitz, D.M., 1996. Skeletal overgrowth and deafness in mice lacking fibroblast growth factor receptor 3. *Nat. Genet.* 12, 390–397.
- Cooke, J., 2004. Developmental mechanism and evolutionary origin of vertebrate left/right asymmetries. *Biol. Rev. Camb. Philos. Soc.* 79, 377–407.
- Creuzet, S., Schule, B., Couly, G., Le Douarin, N.M., 2004. Reciprocal relationships between *Fgf8* and neural crest cells in facial and forebrain development. *Proc. Natl. Acad. Sci. U. S. A.* 101, 4843–4847.
- Crump, J.G., Maves, L., Lawson, N., Weinstein, B., Kimmel, C., 2004. An essential role for Fgfs in endoderm pouch formation influences later craniofacial skeletal patterning. *Development* 131, 5703–5716.
- Deng, C., Wynshaw-Boris, A., Zhou, F., Kuo, A., Leder, P., 1996. Fibroblast growth factor receptor 3 is a negative regulator of bone growth. *Cell* 84, 911–921.

- Draper, B.W., Morcos, P.A., Kimmel, C.B., 2001. Inhibition of zebrafish *fgf8* pre-mRNA splicing with morpholino oligos: a quantifiable method for gene knockdown. *Genesis* 30, 154–156.
- Draper, B.W., Stock, D.W., Kimmel, C.B., 2003. Zebrafish *fgf24* functions with *fgf8* to promote posterior mesodermal development. *Development* 130, 4639–4654.
- Duboc, V., Rottinger, E., Lapraz, F., Besnardeau, L., Lepage, T., 2005. Left–right asymmetry in the sea urchin embryo is regulated by nodal signaling on the right side. *Dev. Cell* 9, 147–158.
- Elizondo, M.R., Arduini, B.L., Paulsen, J., MacDonald, E.L., Sabel, J.L., Henion, P.D., Cornell, R.A., Parichy, D.M., 2005. Defective skeletogenesis with kidney stone formation in dwarf zebrafish mutant for *trpm7*. *Curr. Biol.* 15, 667–671.
- Fisher, S., Halpern, M.E., 1999. Patterning the zebrafish axial skeleton requires early chordin function. *Nat. Genet.* 23, 442–446.
- Fisher, S., Jagadeeswaran, P., Halpern, M.E., 2003. Radiographic analysis of zebrafish skeletal defects. *Dev. Biol.* 264, 64–76.
- Govindarajan, V., Overbeek, P.A., 2006. FGF9 can induce endochondral ossification in cranial mesenchyme. *BMC Dev. Biol.* 6, 7.
- Gower, J.C., 1975. Generalized Procrustes analysis. *Psychometrika* 40, 33–51.
- Hanken, J., Gross, J.B., 2005. Evolution of cranial development and the role of neural crest: insights from amphibians. *J. Anat.* 207, 437–446.
- Hernandez, L.P., 2000. Intraspecific scaling of feeding mechanics in an ontogenetic series of zebrafish, *Danio rerio*. *J. Exp. Biol.* 203, 3033–3043.
- Hibino, T., Ishii, Y., Levin, M., Nishino, A., 2006. Ion flow regulates left–right asymmetry in sea urchin development. *Dev. Genes Evol.* 216, 265–276.
- Iseki, S., Wilkie, A.O., Morriss-Kay, G.M., 1999. *Fgfr1* and *Fgfr2* have distinct differentiation- and proliferation-related roles in the developing mouse skull vault. *Development* 126, 5611–5620.
- Jackman, W.R., Draper, B.W., Stock, D.W., 2004. *Fgf* signaling is required for zebrafish tooth development. *Dev. Biol.* 274, 139–157.
- Kawakami, Y., Raya, A., Raya, R.M., Rodriguez-Esteban, C., Belmonte, J.C., 2005. Retinoic acid signalling links left–right asymmetric patterning and bilaterally symmetric somitogenesis in the zebrafish embryo. *Nature* 435, 165–171.
- Kimmel, C.B., Ullmann, B., Walker, M., Miller, C.T., Crump, J.G., 2003. Endothelin 1-mediated regulation of pharyngeal bone development in zebrafish. *Development* 130, 1339–1351.
- Leamy, L.J., Pomp, D., Eisen, E.J., Cheverud, J.M., 2000. Quantitative trait loci for directional but not fluctuating asymmetry of mandible characters in mice. *Genet. Res.* 76, 27–40.
- Levin, M., 1999. Twinning and embryonic left–right asymmetry. *Laterality* 4, 197–208.
- Levin, M., 2005. Left–right asymmetry in embryonic development: a comprehensive review. *Mech. Dev.* 122, 3–25.
- Marcil, A., Dumontier, E., Chamberland, M., Camper, S.A., Drouin, J., 2003. *Pitx1* and *Pitx2* are required for development of hindlimb buds. *Development* 130, 45–55.
- McIntyre, G.T., Mossey, P.A., 2003. Posteroanterior cephalometric analysis of the parental craniofacial morphology in orofacial clefting. *Cleft Palate-Craniofac. J.* 40, 416–425.
- Miller, C.T., Kimmel, C.B., 2001. Morpholino phenocopies of endothelin 1 (sucker) and other anterior arch class mutations. *Genesis* 30, 186–187.
- Miller, C.T., Schilling, T.F., Lee, K., Parker, J., Kimmel, C.B., 2000. sucker encodes a zebrafish Endothelin-1 required for ventral pharyngeal arch development. *Development* 127, 3815–3828.
- Montero, A., Okada, Y., Tomita, M., Ito, M., Tsurukami, H., Nakamura, T., Doetschman, T., Coffin, J.D., Hurley, M.M., 2000. Disruption of the fibroblast growth factor-2 gene results in decreased bone mass and bone formation. *J. Clin. Invest.* 105, 1085–1093.
- Morriss-Kay, G.M., Wilkie, A.O., 2005. Growth of the normal skull vault and its alteration in craniosynostosis: insights from human genetics and experimental studies. *J. Anat.* 207, 637–653.
- Neff, M.M., Neff, J.D., Chory, J., Pepper, A.E., 1998. dCAPS, a simple technique for the genetic analysis of single nucleotide polymorphisms: experimental applications in *Arabidopsis thaliana* genetics. *Plant J.* 14, 387–392.
- Nie, X., Luukko, K., Kettunen, P., 2006. FGF signalling in craniofacial development and developmental disorders. *Oral Dis.* 12, 102–111.
- Otten, E., 1983. The jaw mechanism during growth of a generalized *Haplochromis* species: *H. elegans*, Trewavas 1933 (Pisces, Cichlidae). *Neth. J. Zool.* 33, 55–98.
- Palmer, A.R., Strobeck, C., 1997. Fluctuating asymmetry and developmental stability: heritability of observable variation vs. heritability of inferred cause. *J. Evol. Biol.* 10, 39–49.
- Potthoff, T., 1984. Clearing and staining techniques. In: Moser, H.G., Richards, W.J., Cohen, D.M., Fahay, M.P., Kendall, A.W., Richardson, S.L. (Eds.), *Ontogeny and Systematics of Fishes*. American Society of Ichthyologists and Herpetologists, Lawrence, Kansas, pp. 35–37.
- Quarto, N., Longaker, M.T., 2005. The zebrafish (*Danio rerio*): a model system for cranial suture patterning. *Cells Tissues Organs* 181, 109–118.
- Reifers, F., Bohli, H., Walsh, E.C., Crossley, P.H., Stainier, D.Y., Brand, M., 1998. *Fgf8* is mutated in zebrafish acerebellar (*ace*) mutants and is required for maintenance of midbrain–hindbrain boundary development and somitogenesis. *Development* 125, 2381–2395.
- Rohlf, F.J., 2005. tpsRelw v1.42. Geometric morphometric software. <http://life.bio.sunysb.edu/morph/soft-tps.html>.
- Rohlf, F.J., Marcus, L.F., 1993. A revolution in morphometrics. *Trend Ecol. Evol.* 8, 129–132.
- Rohlf, F.J., Slice, D., 1990. Extensions of the Procrustes method for the optimal superimposition of landmarks. *Syst. Zool.* 39, 40–50.
- Sagerstrom, C.G., Grimbalt, Y., Sive, H., 1996. Anteroposterior patterning in the zebrafish, *Danio rerio*: an explant assay reveals inductive and suppressive cell interactions. *Development* 122, 1873–1883.
- Shapiro, M.D., Marks, M.E., Peichel, C.L., Blackman, B.K., Nereng, K.S., Jonsson, B., Schluter, D., Kingsley, D.M., 2004. Genetic and developmental basis of evolutionary pelvic reduction in threespine sticklebacks. *Nature* 428, 717–723.
- Shapiro, M.D., Bell, M.A., Kingsley, D.M., 2006. Parallel genetic origins of pelvic reduction in vertebrates. *Proc. Natl. Acad. Sci. U. S. A.* 103, 13753–13758.
- Shimoaka, T., Ogasawara, T., Yonamine, A., Chikazu, D., Kawano, H., Nakamura, K., Itoh, N., Kawaguchi, H., 2002. Regulation of osteoblast, chondrocyte, and osteoclast functions by fibroblast growth factor (FGF)-18 in comparison with FGF-2 and FGF-10. *J. Biol. Chem.* 277, 7493–7500.
- Sobue, T., Naganawa, T., Xiao, L., Okada, Y., Tanaka, Y., Ito, M., Okimoto, N., Nakamura, T., Coffin, J.D., Hurley, M.M., 2005. Over-expression of fibroblast growth factor-2 causes defective bone mineralization and osteopenia in transgenic mice. *J. Cell. Biochem.* 95, 83–94.
- Thisse, C., Thisse, B., Schilling, T.F., Postlethwait, J.H., 1993. Structure of the zebrafish *snail1* gene and its expression in wild-type, *spadetail* and *no tail* mutant embryos. *Development* 119, 1203–1215.
- Tucker, A.S., Yamada, G., Grigoriou, M., Pachnis, V., Sharpe, P.T., 1999. *Fgf-8* determines rostral–caudal polarity in the first branchial arch. *Development* 126, 51–61.
- Valta, M.P., Hentunen, T., Qu, Q., Valve, E.M., Harjula, A., Seppanen, J.A., Vaananen, H.K., Harkonen, P.L., 2006. Regulation of osteoblast differentiation: a novel function for fibroblast growth factor 8. *Endocrinology* 147, 2171–2182.
- Westerfield, M., 1995. *The Zebrafish Book. A Guide for the Laboratory Use of Zebrafish (Danio rerio)*, third ed. Univ. of Oregon Press, Eugene.
- Witten, P.E., Hansen, A., Hall, B.K., 2001. Features of mono- and multinucleated bone resorbing cells of the zebrafish *Danio rerio* and their contribution to skeletal development, remodeling, and growth. *J. Morph.* 250, 197–207.
- Yoon, Y.J., Perkiomaki, M.R., Tallents, R.H., Barillas, I., Herrera-Guido, R., Fong, C.T., Kyrkanides, S., 2003. Association of nasomaxillary asymmetry in children with unilateral cleft lip and palate and their parents. *Cleft Palate-Craniofac. J.* 40, 493–497.
- Yu, K., Xu, J., Liu, Z., Sosic, D., Shao, J., Olson, E.N., Towler, D.A., Ornitz, D.M., 2003. Conditional inactivation of FGF receptor 2 reveals an essential role for FGF signaling in the regulation of osteoblast function and bone growth. *Development* 130, 3063–3074.
- Zuo, J., Jiang, J., Dolce, C., Holliday, L.S., 2004. Effects of basic fibroblast growth factor on osteoclasts and osteoclast-like cells. *Biochem. Biophys. Res. Commun.* 318, 162–167.